Rev. Roum. Sci. Techn.– Électrotechn. et Énerg.
Vol. **69**, *3*, pp. 277–282, Bucarest, 2024

THE EFFECTS OF HYBRID SLIDING MODE LEARNING CONTROL AND FEEDFORWARD ANGLE DROOP CONTROLLER WITH HIGH DROOP GAIN IN HYBRID MICROGRID WITH LOAD UNCERTAINTY AND NONLINEARITY

MOHAMMAD SAEED KOUPAEI NIYA[1]

Keywords: Islanded operation; Angle droop; LCL filter; Hybrid sliding mode controller (HSMC); High droop gain.

The present study proposes a feedforward angle droop strategy based on a discrete-time mathematical model for operation dispatchable distributed generation (DG) units connected directly or through voltage source converters (VSC) to the microgrid. These units should supply their local and common loads. Droop coefficients should be increased to improve power division between different DG units. Also, a time delay in systems' state variables and controller input is a disruptive parameter for the control system's performance. These two parameters have negative effects on network stability. To ensure the stability of the closed-loop system, a predictive sliding mode controller can be used based on discrete-time systems. However, this strategy cannot reduce the chattering phenomenon. This paper discusses the effect of time delay and increases in droop angle coefficients on the whole system and how these impacts can be eliminated. So, a combination of integral sliding mode controller (ISMC), composite nonlinear feedback (CNF), and sliding mode learning control (SMC), which is called hybrid SMC, is used with an angle droop controller.

1. **INTRODUCTION**

Due to modeling errors, parameter changes, and external disturbances, all physical systems are affected by uncertainties. The control of dynamic systems in the presence of uncertainties due to the reduced performance of the controller is a very difficult task that may negatively affect grid stability. So, studies are continuing to develop the controllers to operate in the presence of various uncertainties. The sliding surface should be optimally designed to cover all the limitations and intended features of the control system. In [1], the effects of an angle droop controller on system performance have been studied under load uncertainty, but the effects of an increase in droop gain are not investigated. In [2], the effect of compensator type is investigated in a high-order sliding mode presented. In [3], the effect of ADRC with an angle droop controller is investigated, but the controller's speed is very low. In [4], a linear sliding mode switching function designs the corresponding sliding mode control law, but the effects of the nonlinear condition are not considered. A virtual inertia control based on a new optimal robust controller is proposed in [5] to improve modern power systems' frequency stability and measurement effects. Still, it has yet to be tested for load uncertainties. In addition to the frequency deviation in microgrid, the aspect of controller output signals has also been considered. To eliminate the chattering phenomenon in discrete-time sliding mode control reaching law, a method based on a non-paved controller proposed in [6] can produce high accuracy in SMC. In [7], a nonlinear controller with the help of IOLC and SMC is considered, but the effect of high gain needs to be considered. Implementing SMC through a multi-resonant sliding surface can produce perfect tracking of command references. It can also decrease the total harmonic distortion of converters' output [8]. In [9], the frequency control of microgrids is considered using a genetic algorithm. In practice, the proposed methods may not necessarily guarantee the control stability, robustness, or performance promised by the assumed models. Also, [10] proposed an improved distributed cooperative secondary control strategy to overcome the disadvantages of inherent time delay and achieve either restoration of the voltage amplitude and frequency or active power sharing. However, the effects of nonlinearity are not considered. In [11], another model of SMC has been proposed, in which an internal SMC is used for stable control of current and voltage. It is shown that the controller can track reference commands with high accuracy and within acceptable stability regions. However, it is used only for single-phase converters.

Reference [12] used the adaptive SMC to increase the microgrid's stability. The proposed strategy can control DG units in both grid-connected or islanded modes of operation without any changes in the control structure. However, the control capability is not tested under load current disturbances. Multi-mode performance and transient stability may affect microgrid flexibility. In this condition, the control strategy can be designed based on a three-layer hierarchical structure [13]. In all these papers, there is no significant study on how the gain increase can affect the total operation of the controller system. The current study focuses on problems in the traditional control strategies. It uses a feedforward compensation method besides SMC to change a dynamic interaction between DG units and the network when the droop gain is increased in a hybrid microgrid consisting of a converter base and synchronous DG units. Through changing the contribution of load dynamics, the network stability increases. One of the problems is the impact of load current on the operation of the control system. This study uses a feedforward compensation to remove internal couplings and reduce the impact of load dynamics on the control system. Under these conditions, the closed-loop system shows similar dynamic behavior under no-load and loaded conditions. The present study uses the advantages of the PLL unit, so the need for external frequency measurement is eliminated. The effect of balanced, unbalanced, local, and nonlinear load conditions is addressed, as well as sudden and random load switching incidents and short circuit events on the terminal voltage of a DG unit in the islanded mode operation of a microgrid system.

Moreover, the LCL filter type is used to overcome the harmonics caused by converter switching, and its effects on DG units' performance are investigated. Also, to improve power division between different types of DG units, the droop gain is increased, adversely affecting network stability. A time delay in systems' state variables and controllers' input may cause stability problems in the network. To solve the problem, a combination of adaptive integral sliding mode, composite nonlinear feedback (CNF) for a better control system, and sliding mode learning control for further decreases of the chattering phenomenon is used besides the feedforward angle droop controller.

[1] Faculty of Technology and Engineering, Shiraz Branch, Islamic Azad University, Shiraz, Iran (MS.koupaei@iau.ac.ir)

DOI: 10.59277/RRST-EE.2024.69.3.3

The rest of this paper is organized as follows. Section 2 describes the structure of the islanded network. Section 3 presents the mathematical model for DG units in the islanded mode of operation. Section 4 presents the mathematical structure of the adaptive controller. Section 5 presents simulation results to illustrate the effectiveness of the proposed strategy. Section 6 concludes the paper.

2. ISLANDED NETWORK AND DISTRIBUTED GENERATION STRUCTURE

Figure 1 shows a general configuration of a microgrid that can be used in both connected or islanded from the main grid. The network of Fig. 1 consists of three types of generating units. Two DG units are converter (dispatchable) base units electrically connected to the grid, and the other is a synchronous machine. This unit's output is connected to the main bus (PCC) through transmission lines, which supply four load types. These loads are 1- balanced load, 2- motor load 3-unbalanced load 4-rectified Load. Each DG unit has its local load. Each load can be connected through a transformer to the main bus. In the connected mode of operation, these mentioned loads can be provided by the main grid or shared between DG units and the main grid.

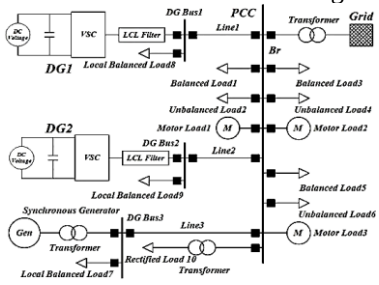

Fig. 1 – General diagram of microgrid.

Figure 2 illustrates the control units of the converter base DG unit. This controller uses a three-phase to two rotating d-q axis system transformation where θ is the axis degree of PLL output concerning the stationary axis α. The three-phase variables Icabc, Igabc, VCabc, VCfabc, and Vtabc, respectively, signify the converter, network side current of the LCL filter, converter side, capacitor voltage of the LCL filter, and PCC bus voltage.

2.1. CURRENT ANGLE DROOP CONTROL STRATEGY WITH LCL FILTER

The current control strategy includes the core shown in Fig. 2. The main purpose of the current controller is the current components' adjustment at the AC side of VSC using pulse width modulation. To analyze how the required pulses are produced in the discrete-time domain, the method expressed in [1] can be used.

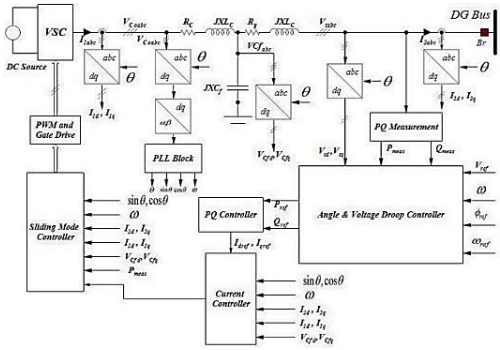

Fig. 2 – Control unit of converter base DG.

3. INTEGRAL ADAPTIVE SLIDING MODE CONTROLLER

SMC, a developed theory of variable structure systems, has attracted much attention due to its robustness against external disturbances and parameter changes. To solve the problem of the chattering phenomenon, a chattering-free integral sliding surface that uses adaptive tuning law can be used. This strategy uses the adaptive law to estimate the unknown parameters. So, knowing the upper bounds of system uncertainty is no longer an essential requirement, and the chattering phenomenon is removed from the control system.

3.1. INTEGRAL SLIDING MODE CONTROLLER

The control signal design process is done in two parts.

- Nominal control design ω_{nom}.
- Design of total control law u.

Initially, nominal control law ω_{nom} is designed. This would ensure the stability of the integral chain in the presence of uncertainty. The total reaching phase can be designed to remove uncertainties and maintain the sliding mode. Consider the following nominal system

$$Z_1^{\bullet} = Z_2,\ \ Z_1^{\bullet} = Z_2,\ldots,\ Z_r^{\bullet} = \omega_{nom}. \quad (1)$$

The main purpose of the controller is to push the state variables of (1) toward $Z = 0$ in finite time. $K_1, K_2, \ldots, K_n$ can be chosen so that the polynomial $(\lambda) = \lambda^n + k_n\lambda^{n-1} + \cdots + k_2\lambda + k_1$ is Hurwitz. Therefore, for (1), there exist $\varepsilon \in (0,1)$ so that for $\alpha_i\epsilon(1-\varepsilon,1),\ i = 1,2,\ldots,n$ feedback system will be stable in finite time [14].

$$\omega_{nom}(Z) = -k_1\text{sign}(Z_1)|Z_1|^{\alpha_1} - k_2\text{sign}(Z_2)|Z_2|^{\alpha_2} - k_n\text{sign}(Z_n)|Z_n|^{\alpha_n},$$
$$\alpha_{i-1} = \frac{\alpha_i\alpha_{i+1}}{2\alpha_{i+1}-\alpha_i}, i = 2,\ldots,n, \text{ with } \alpha_{n+1} = 1. \quad (2)$$

This section develops the reaching control law based on the discontinuous control law. This removes uncertainty from the system, and the control objectives are fulfilled. So, the integral sliding surface can be considered.

$$s(z) = z_n - z_n(0) - \int \omega_{nom}(z)\mathrm{d}t. \quad (3)$$

The derivative of (3) can be obtained as

$$s^{\bullet}(z) = z_n^{\bullet} - \omega_{nom} = \bar{a}(z) + \bar{b}(z)u + \Delta F(z,t) - \omega_{nom}. \quad (4)$$

Using (4) and fixed rate reaching law $s^{\bullet}(z) = -G\text{sign}(S(z))$ [15], the total control rule can be obtained as follows [16].

$$-G\text{sign}\big(s(z)\big) = \bar{a}(z) + \bar{b}(z)u - \omega_{nom}. \quad (5)$$

However, high frequency chattering phenomenon will be existed in control signal. To remove undesired chattering phenomenon on the control input, the adaptive integral sliding mode controller can be used. In the proposed controller, the time derivative of input control $u^{\bullet}$ is used on high derivative order of sliding variables. So instead of using u, the time derivative of input control $u^{\bullet}$ it can be used as input control. The new controller is a discontinuous signal, but its integral is continuous. So, this signal can remove the high-frequency chattering phenomenon. By taking the first-order derivative of (5),

$$u^{\bullet} = -\bar{b}(z)^{-1}(\bar{a}^{\bullet}(z) + \bar{b}^{\bullet}(z)u - \omega_{nom}^{\bullet} + k(z_n^{\bullet} - \omega_{nom}) + \rho\text{sign}(\sigma)) \quad (6)$$

where k is a positive constant and $\rho > |\Delta F^{\bullet}(z,t)|$ considered to fulfill the terms of reaching law $\sigma\sigma^{\bullet} \le -\eta|\sigma|$.

3.2. FREE CHATTERING ADAPTIVE INTEGRAL SLIDING MODE CONTROLLER DESIGN

In practical purposes, upper bound of system uncertainties is unknown and therefore it is difficult to find $\Delta F^{\bullet}(z,t)$ faults. To estimate ρ, the adaptive tuning law can be used. So, the control law of (6) is

$$u^{\bullet} = -\bar{b}(z)^{-1}(\bar{a}^{\bullet}(z) + \bar{b}^{\bullet}(z)u - \omega_{nom}^{\bullet} + k(z_n^{\bullet} - \omega_{nom}) + \hat{T}\text{sign}(\sigma)), \quad (7)$$

where $\hat{T}$ is the estimate of ρ, and can be defined as $\tilde{T} = \hat{T} - T$. $\tilde{T}$ is a parameter that can be estimated by adaptive law $\hat{T}^{\bullet} = v|\sigma|$, where v is a constant positive value.

3.3. CONTROLLER DESIGN BASED ON COMPOSITE NONLINEAR FEEDBACK

Figure 3 shows a block diagram of discrete time integral sliding mode based on CNF. The main purpose of the non-composite nonlinear feedback controller is quick tracking of command input references without generating high overshoot. This can be achieved by combining a discrete-time linear feedback controller with a small damping ratio and a nonlinear feedback controller. The CNF control law is s:

$$u_c(k) = u_L(k) + u_N(k), \quad (8)$$

where $u_L(k), u_N(k)$ respectively represent linear state feedback control and nonlinear feedback law. The general integral sliding mode composite nonlinear feedback control law can be expressed as follows

$$u(k) = Kx(k) + \gamma(r,y)\beta_\tau^{\mathrm{T}}P(\phi + \beta_\tau K)x(k) + (G\beta_\tau)^{-1}(Gx(0) - G\beta_\tau\hat{d}(k) - h(k)) \quad (9)$$

$$\gamma(r,y) = -\rho e^{-\varphi(y-r)^2}, \phi = \phi_\tau + \beta_\tau(G\beta_\tau)^{-1}G$$

$$P = (\phi + \beta_\tau)^{\mathrm{T}}P(\phi + \beta_\tau) + R, \quad (10)$$

where y, r are input and output references. Also $\rho > 0$, $\varphi > 0$ are tuning parameters.

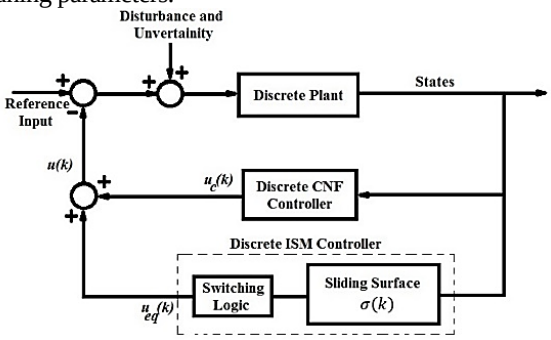

Fig. 3 – Block diagram of the discrete-time composite nonlinear feedback based on integral sliding mode controller.

3.4. LEARNING SLIDING MODE CONTROLLER

An integral sliding mode controller can be combined with other control strategies to achieve a free-chattering controller. The previous section expressed a new strategy: combining ISMC with CNF. This part introduces the integral sliding mode composite nonlinear feedback controller based on the learning controller for a class of uncertain dynamic systems. It can be shown that the proposed strategy can guarantee the stability of the closed-loop system. The principles of controller design are as follows. The sliding variable can be expressed as follows

$$s(t) = Cx(t) \quad (11)$$

where $C \in R^{1\times n}$ is a matrix of sliding mode parameters. The time derivative of (11) can be expressed as follows

$$S^{\bullet}(t) = f(t) + bu(t),$$

$$f(t) = \sum_{i=1}^{n-1} c_i x^{(i)}(t) + f(x,t) + d(t). \quad (12)$$

The learning sliding mode controller can be obtained as

$$u(t) = u(t-\tau) - \Delta u(t), \quad (13)$$

where $\Delta u(t)$ represents a correction component, and it is expressed as follows

$$\Delta u(t) = \begin{cases} \frac{1}{bs(t)}\left(\alpha\widehat{V^{\bullet}}(t-\tau) + \beta\left|\widehat{V^{\bullet}}(t-\tau)\right|\right) & \text{for } s(t) \neq 0 \\ 0 & \text{for } s(t) = 0 \end{cases} \quad (14)$$

where $\alpha, \beta > 0$ are control parameters, $\widehat{V^{\bullet}}(t-\tau)$ approximates $V^{\bullet}(t-\tau)$, τ – time delay and $V^{\bullet}(t)$ is a first order derivative of Lyapunov function. $V(t) = 0.5s(t)^2$ can be selected as a Lyapunov function for the close loop system.

4. CONTROLLER DESIGN

4.1. MODEL OF VOLTAGE SOURCE CONVERTER WITH LCL FILTER

A voltage source converter with an LCL filter is considered to implement control strategies expressed in previous sections [1, 2].

4.2. THE PROCESS OF CONTROLLER DESIGN

To begin the process of learning ISMC design, the continuous state equations of Fig. 4 obtained as follows

$$x^{\bullet} = Ax + Bu, y = Cx + Du \quad (15)$$

where $u \in R$ input control vector and $x \in R^3$ represents the state variable vector, and it is considered as $x = [i_c \quad i_g \quad v_c]^{\mathrm{T}}$.

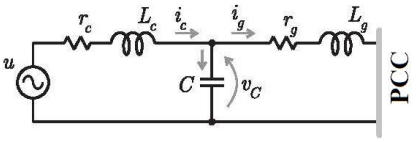

Fig. 4 – A simplified model of source with LCL filter.

According to Fig.4 the A, B, C, D matrixes can be considered as

$$A = \begin{bmatrix} -\frac{r_c}{L_c} & 0 & -\frac{1}{L_c} \\ 0 & -\frac{r_g}{L_g} & -\frac{1}{L_g} \\ \frac{1}{C} & -\frac{1}{C} & 0 \end{bmatrix}, B = \begin{bmatrix} \frac{1}{L_c} \\ 0 \\ 0 \end{bmatrix},$$

$$C = [1 \quad 1 \quad 0], \; D = [0] \quad (16)$$

$$A_d = \begin{bmatrix} 1 - \frac{Tr_c}{L_c} & 0 & -\frac{T}{L_c} \\ 0 & 1 - \frac{Tr_g}{L_g} & -\frac{T}{L_g} \\ \frac{T}{C} & -\frac{T}{C} & 0 \end{bmatrix}, B_d = \begin{bmatrix} \frac{r_g + L_c\left(\frac{r_c}{L_c} - 1\right)}{L_c(r_c + r_g)} \\ \frac{r_c - L_c\left(\frac{r_c}{L_c} - 1\right)}{L_c(r_c + r_g)} \\ -\frac{r_c r_g - L_c L_g\left(\frac{r_c}{L_c} - 1\right)}{L_c(r_c + r_g)} \end{bmatrix}, \quad (17)$$

where parameter T represents the sampling period of the signal. Considering the time delay of state variable parameters and control input is the main contribution of the proposed controller. Therefore, by considering the time delay, the new state equations can be expressed as:

$$\bar{x}(k+1) = \bar{G}\bar{x}(k) + \bar{H}u(k), y(k) = \bar{C}\bar{x}(k) \quad (18)$$

where $\bar{x} = [x \quad u_d]^T$. In this vector u_d is a new state variable that reflects the time delay in digital applications. Therefor the new matrixes $\bar{G}, \bar{H}, \bar{C}$ can be obtained as follows

$$\bar{G} = \begin{bmatrix} B_d & A_d \\ 0 & 0 \end{bmatrix}, \bar{H} = \begin{bmatrix} 0 \\ 0 \\ 0 \\ 1 \end{bmatrix}, \bar{C} = [C \quad 0]. \quad (19)$$

5. CASE STUDY AND THE RESULTS OF THE SIMULATION

To demonstrate the effectiveness of the proposed control strategy, Fig. 1 with switching details has been simulated in Digsilent Power factory environment. The microgrid of Fig. 1 can be used in both islanded and grid-connected modes of operation. Parameters of lines and DG units used in the microgrid of Fig.1 are presented in Table 1. Values for each load in Fig. 1 are given in [2]. In Fig. 1, each DG unit has its local loads, which can be provided by its producers or divided between DG units according to their droop coefficient. In this paper, the latter is selected.

Table 1

DG units and Line parameters used in microgrid

DG Parameters			
Parameter	DG #1	DG #2	DG #3
m (p.u)	0.167	0.2	0.1333
n (p.u)	0.333	0.4	0.267
S (kva)	120	100	150
Voltage (V)	400	400	200
Line Parameter	**Line**	**Line 1**	**Line 2**
R(Ω/Km)	0.1	0.1	0.1
XL(Ω/Km)	0.02	0.02	0.02
Length(km)	2	3	4
Voltage(V)	400	400	400

The series of events investigated in this microgrid are given in Table 2.

Table 2

Series of events investigated in microgrid

Item	**Event type**	**Time (sec)**
1	Disconnecting from main grid	5
2	Operation of controller	5
3	Connecting rectified load	50
4	Connecting motor loads (M1,M2,M3)	80
5	Connecting Load2 & Load4 & Load6	140
6	Three phase short circuit event in line 1	200
7	Disconnecting Line 1 from the microgrid	200.07
8	Disconnecting unbalanced Load 2 – 4 - 6	250-280-300
9	Disconnecting rectified Load	320
10	reconnecting Line 1 to microgrid	450
11	Connecting Local Load7 , 8 and 9	550 – 600 – 650

5.1. SYSTEM RESPONSE IN THE PRESENCE OF CONVENTIONAL ANGLE DROOP CONTROLLER WITH HIGH DROOP GAIN COEFFICIENTS

To optimize load sharing between DG units of Fig.1, droop coefficients will be increased. In this case, as Fig.5 shows, the network becomes unstable. To solve this problem, the proposed controller can be used with an angle droop controller.

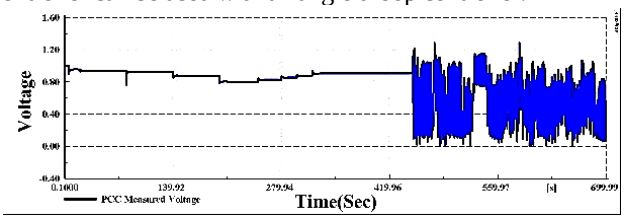

Fig. 5 – PCC measured voltage without the proposed controller.

5.2. MODE TRANSFER OF MICROGRID

According to Table 3 at t = 5 s, a transition will occur from the grid connected to the islanded mode of operation. Only balanced loads are connected to the grid during the transition from grid-connected to islanded mode. Figure 6 shows the PCC-measured voltage and frequency in the case of the proposed controller. Also, Fig.7 shows active and reactive power sharing between the DG units. This figure shows that active and reactive power is divided between the DG units based on the DG units' droop coefficients.

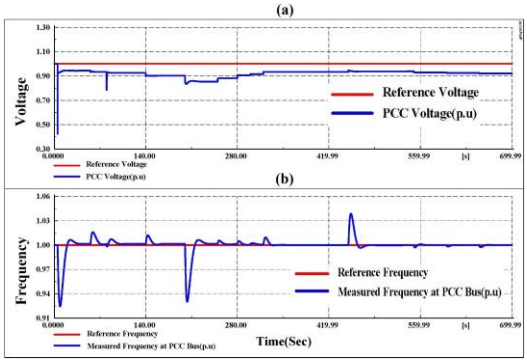

Fig. 6 – a – PCC measured voltage; b – PCC measured frequency.

5.3. RESPONSE TO LOAD CURRENT DISTURBANCE

One type of load considered in Fig. 1 is a rectified Load, a three-phase full-wave rectifier circuit using thyristors as the switching element. The rectifier is switched on at t = 50 s in this case study. Due to thyristor switching, total harmonic distortion (THD) of voltage and current at the PCC bus will be increased. Figure 8 shows the THD of PCC voltage with the proposed controller and high droop gain. As Fig. 8 shows, the average THD of PCC Voltage is about 0.8 %, which is lower than that of normal THD.

5.4. MOTOR AND UNBALANCED LOAD CONDITION

To investigate the system response in the case of induction motor loads, this paper switches the motor loads on at t = 80 s. It should be noted that the balanced and rectified loads are still connected to the grid. As Fig. 7 shows, despite load imbalance at t = 140 s, the DG units generate a symmetrical voltage, and loads are also divided between the DG units according to their respective droop coefficients, as shown in Fig. 8a. Figure 8b illustrates the ratio of the negative to the positive-sequence components (*i.e.*, VPCCNeg / VPCCPos) of PCC bus voltage with a proposed controller with high droop gain. As Fig. 8a shows, the ratio of the negative to positive sequence component of the PCC bus goes to zero with every change in condition with the proposed control strategy.

At t = 200 s, a three-phase short circuit occurs at the line connected to the DG unit#1 while the loads mentioned in sections 1 to 4 are still connected to the grid. This transmission line is disconnected from the grid after 0.07 seconds (*i.e.*, t = 200.07 s). From t = 200.07 s, DG units #2 and #3 are responsible for providing power demand and maintaining the voltage and frequency of the grid. After fault clearing, the PCC voltage drop to provide the required reactive power of the grid. Loads are divided between the DG units according to their respective droop coefficients. Also, during the DG unit #1 outage, other units operate at very high levels of power generation to maintain the voltage and frequency of the DG units at their respective references.

Therefore, load shedding should be done to reduce power generation. This happened at t = 250 s, 280, 300, and 320, which disconnected Load 2, Load 4, and Load 6 and rectified Load from the grid. As Figs. 6–8 show, by reconnecting line 1 at t = 450 s, the proposed control strategy forced the generated voltage and frequency of DG units to track their respective references.

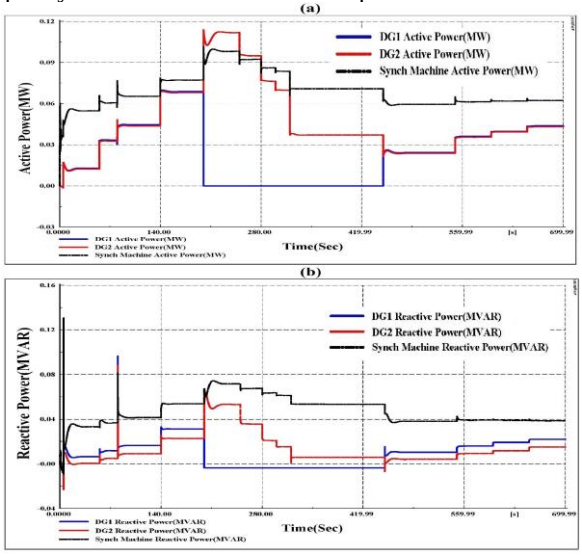

Fig. 7 – a –Active power sharing between DG units;
b – Reactive power sharing between DG units.

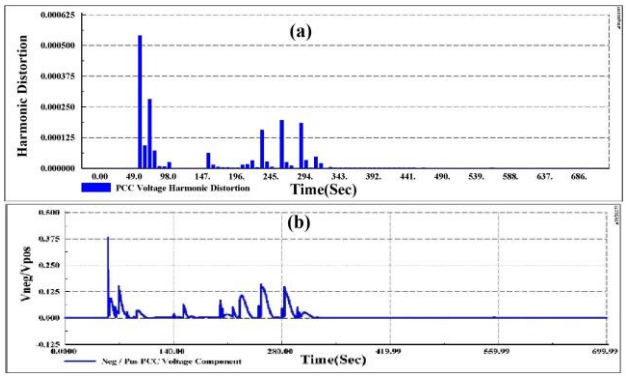

Fig. 8 – a – Total harmonic distortion of PCC voltage;
b – Overall *VPCCNeg / VPCCPos* ratio.

5.5. SHORT CIRCUIT EVENT

At t = 200 s, a three-phase short circuit occurs at the line connected to the DG unit#1 while the loads mentioned in section A are still connected to the grid. This transmission line is disconnected from the grid after 0.07 s (*i.e.*, t = 200.07 s), isolating DG unit #1 from the grid. From t =2 00.07 s, DG units #2 and #3 are responsible for providing power demand and maintaining the voltage and frequency of the grid. As Fig. 9 shows, after fault clearing, the generated voltage of DG unit #3 drops to provide the required reactive power of the grid. Loads are divided between the DG units according to their respective droop coefficients. Also, during the DG unit #1 outage, other units operate at very high levels of power generation to maintain the voltage and frequency of the DG units at their respective references. Therefore, load shedding should be done to reduce power generation. This happened at t = 250, 280, 300, and 320 s, disconnecting Load 2, Load 4, Load 6, and rectifying Load from the grid. As Figs. 9, 10 show, by reconnecting line 1 at t = 450 s, the proposed control strategy forced the generated voltage and frequency of DG units to track their respective references.

5.6. RESPONSE TO CONNECTED/DISCONNECTED MODE OF OPERATION IN A LARGE GRID

To test the proposed controller in an islanded or grid-connected mode of operation in a large network, the IEEE 33-bus test distribution system is selected. Figure 10 shows the IEEE 33-bus test distribution system [17]. Tables 3 and 4 show the parameters of the DG unit in Fig. 11 and the series of events in a microgrid. According to the conditions and issues stated above, Fig. 12 shows the active and reactive power generated by the DG units. Figure 13 illustrates the voltage and frequency of bus #1 in the presence of the proposed control strategy.

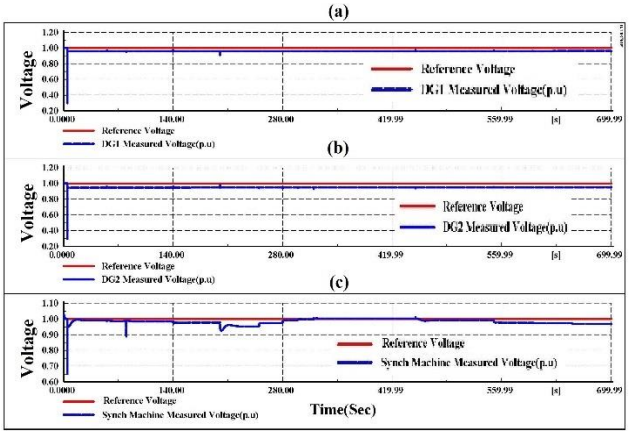

Fig. 9 – Generated voltage of DG units: a – DG #1; b – DG#2; c – synch generator in SC event.

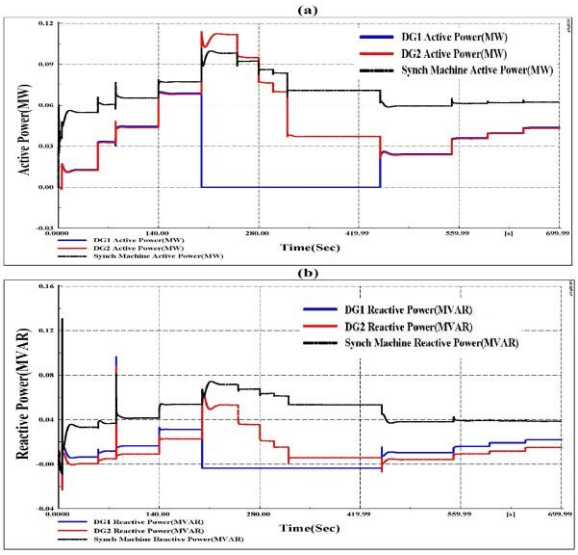

Fig. 10 – a – Active power sharing between DG units in SC event;
b – Reactive power sharing between DG units is needed in SC events.

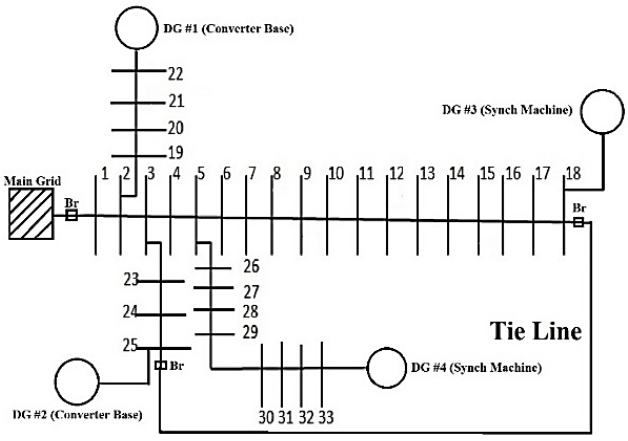

Fig. 11 – The IEEE 33-bus test distribution system.

Table 3

DG unit parameters used in the IEEE 33-bus test

DG Parameters				
Parameter	**DG #1**	**DG #2**	**DG #3**	**DG #4**
m (p.u)	0.167	0.2	0.1333	0.08
n (p.u)	0.333	0.4	0.267	0.16
S (mva)	1.2	1	1.5	2.5
Voltage (kV)	33	33	6	6

Table 4

Series of events investigated in 33 bus IEEE microgrid

Item	Event type	Time
1	Disconnecting from main grid	5
2	Operation of controller	5
3	Disconnecting DG #2 from the microgrid	40
4	Disconnecting Line between bus 2 & 23	40
5	Connecting line between bus 18 & 25	50
6	Connecting DG #2 to the microgrid	100
7	Connecting Line between bus 2 & 23	100
8	Disconnecting line between bus 18 & 25	100
9	Connecting microgrid to the main grid	150
10	Disconnecting from main grid	200
11	Decreasing impedance of line bus 6-7 & 2-19	220
12	Increasing impedance of line between bus 10-11 & 29-30	220

The results of these figures show the effectiveness of the proposed method in a large microgrid and illustrate good performance in the transition from grid-connected to islanded mode of operation.

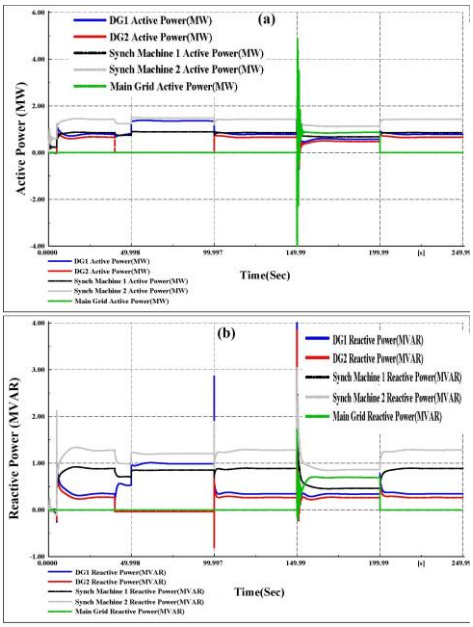

Fig. 12 – a – Active power; b – Reactive power sharing between DG units and main grid in a large network.

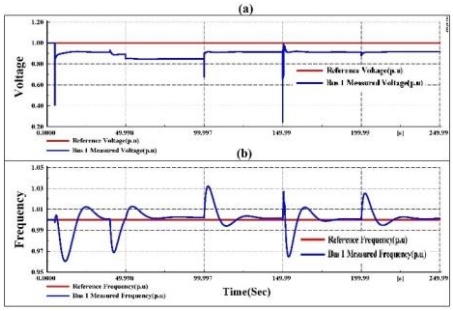

Fig. 13 – a – Variation of Bus #1 voltage; b – Frequency in different events.

The results show that the proposed control strategy responded adequately to all these various types of loads and events and increased droop gain (which is not considered in other types of work). Therefore, the results clearly show the effectiveness of this controller in different conditions.

6. CONCLUSION

The current study proposed an angle droop controller combined with adaptive integral sliding mode, Composite Nonlinear Feedback (CNF), and Sliding Mode Learning Control for converters of dispatchable DG units connected to the network in discrete time domain to ensure proper load sharing and stable performance of DG units in increased droop gain. This study proposed a combination of different types of DG units in microgrids. Two DG units are converter base units, and one is a synchronous machine. Also, the current study considered the effect of time delay on the system's total performance. Therefore, combining adaptive integral sliding mode, CNF, and SMLC eliminates time delay effects. Various types of loads, including induction motor load, unbalanced load, load current disturbance, and local loads, are considered to demonstrate the effectiveness of the proposed control strategy. This strategy ensures proper load sharing between all DG units by utilizing the current controller with an angle droop controller in all the loads. An LCL-type filter eliminates harmonics produced by the interface converters. The presented study uses the advantages of a PLL unit, so the need for external frequency measurement is eliminated. It can also set up a control strategy with unusual circumstances and show robust properties in different switching conditions. The performance of the proposed control strategy was tested for different conditions in an islanded microgrid. Also, the proposed control strategy demonstrated good performance in large and transition from grid-connected to islanded mode of operation. The overall effectiveness of the proposed control strategy was studied in detail with several loads and transient conditions.

Received on 26 April 2023

REFERENCES

1. M. Niya, A. Kargar, S. Derakhshandeh, *Effects of an angle droop controller on the performance of distributed generation units with load uncertainty and nonlinearity*, Journal of Power Electronics, **17**, *2*, pp. 551–560 (2017).
2. M.S.K Niya., A. Kargar, S.Y. Derakhshandeh, *Effects of angle droop and controller type in hybrid microgrid with load uncertainty and nonlinearity*, Rev. Roum. Sci. Techn. – Électrotechn. et Énerg., **62**, *3*, pp. 233–239 (2017).
3. M.S.K. Niya, *The effects of adaptive repetitive controller and feedforward angle droop controller with high droop gain in hybrid microgrid with load uncertainty and nonlinearity*, Rev. Roum. Sci. Techn. – Électrotechn. et Énerg., **64**, *2*, pp. 149–155 (2019).
4. Y. Cao *et al*., *Sliding mode control for uncertain fractional-order reaction-diffusion memristor neural networks with time delays*, Neural Networks, p. 106402 (2024).
5. H. Ali, G. Magdy, D. Xu, *A new optimal robust controller for frequency stability of interconnected hybrid microgrids considering non-inertia sources and uncertainties*, International Journal of Electrical Power & Energy Systems, **128**, p. 106651 (2021).
6. H. Du *et al*., *Chattering-free discrete-time sliding mode control.* Automatica, **68**, p. 87-91 (2016).
7. K. Mendaz, M. FliTTI, *Input-output linearization control based on the sliding mode of the squirrel cage motor*, Rev. Roum. Sci. Techn. – Électrotechn. et Énerg., **68**, *2*, pp. 176–181 (2023).
8. X. Hao *et al*., *A sliding-mode controller with multiresonant sliding surface for single-phase grid-connected VSI with an LCL filter*, IEEE Transactions on Power Electronics, **28**, *5*, pp. 2259–2268 (2013).
9. G.K. Suman, J.M. Guerrero, and O.P. Roy, *Stability of microgrid cluster with Diverse Energy Sources: A multi-objective solution using NSGA-II based controller*, Sustainable Energy Technologies and Assessments, **50**, p. 101834 (2022).
10. W. Sun *et al*., *Distributed controller design and stability criterion for microgrids with time-varying delay and rapid switching communication topology*, Sustainable Energy, Grids and Networks, **29**, p. 100566 (2022).
11. S.K. Gudey, R. Gupta, *Sliding-mode control in voltage source inverter-based higher-order circuits*, International Journal of Electronics, **102**, *4*, pp. 668–689 (2015).
12. X. Su *et al*., *Microgrid stability controller based on adaptive robust total SMC*, Energies, **8**, *3*, pp. 1784–1801 (2015).
13. Q. Zhang *et al*., *A multi-mode operation control strategy for flexible microgrid based on sliding-mode direct voltage and hierarchical controls*, ISA transactions, **61**, pp. 188–198 (2016)
14. D. Yan, S. Jianhui, S. Yong, *A unified power controller for photovoltaic generators in microgrid* in *electric utility deregulation and restructuring and power technologies (DRPT)*, 4th International Conference on, IEEE, 2011.
15. G. Bartolini *et al*., *On multi-input chattering-free second-order sliding mode control*, IEEE Transactions on Automatic Control, **45**, *9*, pp. 1711–1717 (2000).
16. W. Gao, J.C. Hung, *Variable structure control of nonlinear systems: a new approach*, IEEE Transactions on Industrial Electronics, **40**, *1*, pp. 45–55 (1993).
17. K. Dharageshwari, C. Nayanatara, *Multiobjective optimal placement of multiple distributed generations in IEEE 33 bus radial system using simulated annealing*, International Conference on Circuits, Power and Computing Technologies (ICCPCT), IEEE, 2015.